RSC Advances

Ultrasmall superparamagnetic Ni nanoparticles embedded in polyaniline as a lightweight and thin microwave absorber

SCHOLARONE™
Manuscripts

RSC Advances

Dynamic Article Links ▶

PAPER

Ultrasmall superparamagnetic Ni nanoparticles embedded in polyaniline as a lightweight and thin microwave absorber

Dandan Han,*[a] Ningru Xiao,[b] He Hu,[c] Bao Liu,[a] Gengxin Song,[a] and He Yan[a]

   In this work, we have reported on the preparation and the lightweight and thin microwave absorbent application of ultrasmall Ni nanoparticles embedded in polyaniline (PANI). Ni nanoparticles have the averaged diameter of 2.1 nm, which are single crystals and possess the single magnetic domain structure. The blocking temperature of Ni@PANI nanocomposite is established to 52 K. The Ni@PANI
10 nanocomposite is in superparamagnetic state at 300 K. The optimal reflection loss value of paraffin-bonded composite with 25 wt% Ni@PANI nanocomposites reaches -22.98 dB at 17.8 GHz corresponding to the thickness of 1.0 mm. Compared with the represented Ni-based nanocomposites, Ni@PANI nanocomposites possess the favorable properties in a lower density and thinner thickness, resulting from the combined effect of magnetic loss and dielectric loss by introducing ultrasmall superparamagnetic Ni
15 nanoparticles into PANI matrix.

1. Introduction

   With the development of electronic and communication technology, electromagnetic (EM) pollution has become one of the emerging issues in succession of air pollution, water
20 contamination and noise pollution. Hence, it is of great importance to absorb the EM wave radiation around us. EM wave absorber, which can absorb the EM wave energy and transfer it to the heat energy, effectively solve the above problem.[1-4] The desired EM wave absorbers with favorable properties in a wide
25 frequency range, strong absorption, a low density and thin thickness have already attracted a great deal of attention from all over the world.[5-7] Compared with the conventional ferrites, metal magnetic nanoparticles are quite suitable as EM wave absorbers because of small size, large specific surface area, and more
30 dangling chemical bonds, which might lead to the interface polarization and the activation of nanoparticles.[8] However, each kind of nanoparticles just has its intrinsic properties. To develop the advanced EM absorber, the composite nanoparticles may be an efficient strategy. Some nanocomposites, including Fe@C,
35 Ni@C, Ni@ZnO, Co@C, CoNi@C, FeCo@C, Ni@(C, silicides), Fe@Sn oxides, Ni@Cu oxides,[9-17] etc., have been prepared and been investigated as the microwave absorber. Compared with Fe (240-620) and Co (174), Ni possesses the higher relative permeability (1120), which can lead to the better magnetic loss.
40 Ni-based nanocomposites, such as Ni@C, Ni@polyaniline, Ni@carbon nanotubes, Ni@Ag, Ni@graphene, and Ni@Fe₃O₄,[10,18-22] have been widely investigated as the microwave absorber. However, the reported nanocomposites mainly exhibit strong absorptions with thick absorbing thickness (> 2.0 mm). In
45 addition, the high weight of Ni becomes an obstacle to the practical use of the above Ni-based nanocomposites.
   Adding magnetic nanoparticles into conducting polymer

matrix to prepare the composite is another way to enhance microwave absorption performance of magnetic nanoparticles.
50 The polymer matrix act not only as a center of interfacing polarization but also as an insulating matrix between the magnetic particles, give rise to the enhanced dielectric loss and good impedance match.[23-26] It also reduces the weight and the thickness of nanocomposites-based absorbers realizing the
55 demand of microwave absorbers with high-efficiency absorption and low-weight and thin-thickness. [27] The microwave absorption behavior of core-shell structured poly(3,4-ethylenedioxy thiophene)-barium ferrite nanocomposites and Fe₃O₄/polypyrrole core/shell structured nanocomposites have been investigated in
60 detail.[25,26] The high cost and complex preparation process of poly(3,4-ethylenedioxy thiophene) and polypyrrole restricted their application in microwave absorber. Among the conducting polymers, polyaniline (PANI) is particularly interesting for its high conductivity, easy synthesis, low cost, and good
65 environmental stability. PANI is unique for its tunable electrical conductivity.[23] Some PANI-based nanocomposites, including Fe₃O₄@PANI, Co@C@PANI, PANI@graphene oxide@Fe₃O₄, Ni₀.₆Zn₀.₄Fe₂O₄@PANI, PANI@magnetite, etc., have been synthesized and their microwave absorption have been
70 investigated in detail.[28-32]
   Ultrasmall nanoparticles, with sizes in the 1-3 nm range, exhibit unique properties distinct from free molecules and larger sized nanoparticles.[33] The ultrasmall nanoparticles usually exhibit a single-domain size and become superparamagnetic above a
75 certain (blocking) temperature T_B.[33] Such nanoparticles behave like paramagnetic systems with large magnetic moment, fast reaction response to the applied magnetic field, and no remanence,[34] which are beneficial for the enhanced microwave absorption abilities. Liu et al prepared the superparamagnetic

FeNi$_3$ nanoparticles and ferromagnetic FeNi$_3$ nanoparticles, respectively, and proved that the microwave absorption ability of superparamagnetic FeNi$_3$ nanoparticles was enhanced, as seen from not only the high reflection loss but also the wide effective absorption band width at the same thickness.[35]

Therefore, the synthesis of ultrasmall superparamagnetic Ni nanoparticles embedded in PANI nanocomposites is imperative if it is to be used as the lightweight and thin microwave absorber. In this work, superparamagnetic Ni nanoparticles embedded in PANI nanocomposites have been prepared by a simple oxidation-reduction method followed by an in situ polymerization process. The structure, morphology, magnetic properties, complex permittivity and permeability, and EM wave absorption of the nanocomposites are investigated in detail.

2. Experimental

2.1 Materials

Nickel (II) nitrate hexahydrate (Ni(NO$_3$)$_2$·6H$_2$O), hydrazine hydrate (N$_2$H$_4$·H$_2$O), sodium hydroxide (NaOH), dodecyl benzenesulfonic acid (ABS), aniline, polyethylene glycol, cyclohexane and ammonium persulfate ((NH$_4$)$_2$S$_2$O$_8$) were obtained form Jilin Chemical Company (Jilin, China). All chemicals were of analytical grade and used without further purification. Distilled water was used in all experiment process.

2.2 Synthesis of Ni@PANI nanocomposites

Firstly, a solution was prepared by dissolving 8.73g Ni(NO$_3$)$_2$·6H$_2$O, 24 ml polyethylene glycol, 3 ml cyclohexane and 1.2 g NaOH in 100 mL distilled water. Subsequently, a 20 mL volume of N$_2$H$_4$·H$_2$O (85 wt%) was added to the solution. The mixture was stirred vigorously until it was homogeneous. Then, 1 ml of ABS was added into the above solution under constant stirring. Afterward, 4 ml of HCl (1 mol/L) and 4 ml of aniline monomer were added into the above mixture. Finally, the prepared solution was put into two flasks with continual stirring in ice-water bath (0 °C). Concurrently, an aqueous solution of 3 g of (NH$_4$)$_2$S$_2$O$_8$ and 4 mL of HCl (1 mol/L) dissolved in 100 mL distilled water as an oxidizing agent was gently added to the above mixture. This process continued for 2 h to complete polymerization reaction. After the mixture was under stirring for 10 h, the precipitate were filtered and thoroughly washed with acetone several time and then dried in vacuum at 70 °C for 4 h, which could obtain the Ni@PANI nanocomposites.

2.3 Materials characterizations

The composition and phase purity of the as-prepared sample were analyzed by X-ray diffraction (XRD, Brucker D8 Advance) at 40 kV voltage and 50 mA current with Cu K$_\alpha$ radiation (λ=1.5418 Å). Fourier transform infrared spectroscopy (FTIR) spectrum was recorded on Perkin-Elmer FTIR spectrophotometer (450-2000 cm^{-1}) with a 4.0 cm^{-1} resolution. High-resolution transmission electron microscopy (HRTEM) image was obtained on a JEOL-2010 transmission electron microscopy at an acceleration voltage of 200 kV. X-ray photoelectron spectroscopy (XPS) was used to determine the elements' chemical states and the valance band spectrum. Thernogravimetric analysis (TGA, NETZSCH STA 449 F3 apparatus) was performed in air with a heating rate of 5 °C min^{-1}. The magnetic properties were

determined with a commercial Superconducting Quantum Interference Device magnetometer (VSM-SQUID).

The composite sample used for EM absorption measurement was prepared by mixing Ni@PANI nanocomposites with paraffin, which was described in detail elsewhere.[1-15] The amount of nanoparticles in the paraffin-bonded composite is usually in the 30%-60%. In order to prove the present system as a lightweight and thin microwave absorber, the amount of nanoparticles is established to be 25 wt%. The complex permittivity and permeability of the composites were measured by an Anritsu 37269D vector network analyzer using the coaxial method.

3. Results and Discussion
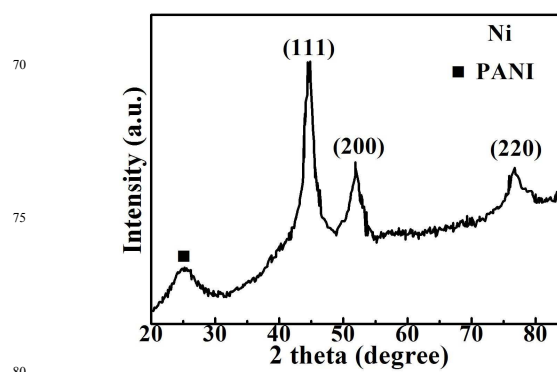
Fig.1. XRD pattern of as-prepared Ni@PANI nanocomposite.

Fig.1 presents XRD pattern of Ni@PANI nanocomposite. Fig.1 reveals that the sharp peaks of (111), (200) and (220) in nanocomposites are corresponding to typical face centered cubic structure of Ni phase (JCPDS cards No.65-0380). The broad peak located at 25.1^o is typical for PANI, ascribed to the perpendicular periodicity of the part PANI chains and the amorphous nature of the other PANI.[36] The absence of impurity peaks in the XRD pattern indicates that the synthesized nanocomposites have a high degree of purity. The crystal size D of the Ni nanoparticles can be calculated using Debye-Scherer formula, $D=0.89\lambda/\beta cos\theta$, where λ is 1.5418 Å and β is the half maximum of the diffraction peak corresponding to the Bragg's angle θ.[37] The calculated D of the Ni nanoparticles is 3.2± 1 nm.

The morphology and microstructure of the as-prepared Ni@PANI nanocomposite are characterized using TEM. As shown in Fig. 2(a), Ni nanoparticles (black dots) are embedded in the amorphous framework (PANI matrix). Based on 100 particles for determining the distribution, the size distribution of Ni nanoparticles is shown in the inset of Fig.2 (a), ranging from 1 to 5 nm. According to the measurement of more than 100 particles, the average diameter of Ni nanoparticles is observed to be 2.1 nm. Note that the value consists with the calculated D form the XRD pattern. A single particle can be composed of several crystals. The average diameter is slight lower than the calculated crystal size. Each Ni nanoparticle should possess the single crystal. A magnetic particle that stays in a single domain state for all magnetic fields is called a single domain particle. The magnetic domain is independent of the crystal size. Taking into account that the magnetic single domain of Ni is ~ 55 nm, [11, 12] the as-prepared Ni nanoparticles are single crystals and possess the

single magnetic domain structure. The HRTEM image of a nanoparticle in Fig. 2(b) exhibits the good crystallinity and shows the clear lattice fringes corresponding to a group of atomic, confirming its crystalline nature. The distance between the lattice fringes is 0.2 nm, which agrees with interplanar spacing of the (111) plane of Ni. The ultrasmall Ni nanoparticles easily drift under the HRTEM. It is difficult to capture the clear HRTEM images. As shown in Fig.2(c), the selected area electron diffraction (SAED) is mainly composed of concentric diffraction rings, revealing the crystal nature of Ni nanoparticles. The rings are indexed out, which are well coincident with Ni in XRD. The amorphous ring in Fig.2(c) corresponds to the PANI. In order to determine the valence state of Ni, XPS spectrum was measured after etching time of 10 s. The XPS spectrum of the Ni2p is shown in Fig.2(d). The binding energies of 852.8 and 870 eV correspond to the Ni2p3/2 and Ni2p1/2 electron states in metallic Ni, [38, 39] while the weak peak at 859.4 eV indicates the satellite peak of Ni2p3/2.[40] It is worthy noted that a weak peak appears at 854.2 eV, indicative of the existence of a small amount of NiO.[41]

TGA was employed to determine the content of PANI in Ni@PANI nanocomposites. In Fig.3(a), the weight loss below 100 ^oC could be attributed to the evaporation of adsorbed moisture.[42] The rapid weight loss at high temperature covers up the truth of the oxidation from Ni to NiO. According to the weight loss of Ni@PANI nanocomposites, the content of PANI in the composites is calculated to be about 53 %. FTIR spectroscopy is used to determine the chemical structure of the Ni@PANI nanocomposites. The FTIR spectra of pure PANI and Ni@PANI nanocomposites are given in Fig. 3(b). Compared with the curve of pure PANI, the characteristic peaks of PANI (at 1554, 1470, 1298, 1097 and 802 cm^{-1}) are clearly observed in the curve of Ni@PANI nanocomposites.[37,43] Besides the above peaks, a new peak at about 598 cm^{-1} is attributed to Ni-Ni stretching vibration, indicating the presence of Ni nanoparticles and PANI in the nanocomposites. The FTIR spectrum of the Ni@PANI nanoparticles exhibits a clear blue shift with respect to that of PANI, indicating that the aniline molecule may be in contract with the Ni nanoparticles by coordinating interactions between the magnetic ions and aniline during the polymerization process.[44]

Fig.4(a) shows the typical magnetization (*M*) versus temperature (*T*) measurements at an applied field (*H*=100 Oe) after different cooling process (at 5-300 K) for as-prepared nanocomposites. The temperature dependence of the magnetization was determined in both field cooling (FC) and zero field cooling (ZFC) regimes. In the ZFC case, the sample was first cooled in zero magnetic field to 5 K and then a magnetic field of 100 Oe was applied to the samples. In such a ZFC condition, the measurements were performed upon heating up to 300 K. The FC data were obtained within the same temperature range after cooling the sample in the same field.[45] From Fig.4(a), it can be clearly seen that a peak appears at 52 K in the ZFC curve, indicating the blocking temperature T_B.[46] T_B is determined by many factors, such as the diameter distribution of nanoparticles, the applied magnetic field and the measuring time, etc. Let us now discuss why useful information can be obtained from the ZFC and FC magnetization data. It should be noted that the net magnetization is zero, i.e. the sample is at the equilibrium

state, before a magnetic field is applied to the sample in the ZFC measurement. After a low field is applied, the equilibrium is broken due to the Zeeman energy. When energy barriers exist in the system, the sample cannot reach the corresponding thermodynamic equilibrium state at such a low temperature and a low field, and the system will try to approach the corresponding equilibrium state slowly through relaxation processes. With increasing the temperature, the relaxation rate increases exponentially and the magnetic moments of more and more particle will turn to the field direction, i.e., the magnetization of samples increase with temperature. At a certain temperature, the magnetization increases to the value of the equilibrium state. If the temperature increases further, it then decreases following the Curie law, and consequently a maximum appears at T_B. So if the applied field increases, magnetization increases to the value of the equilibrium state at the lower temperature.[47] As referred in Ref [48], the applied magnetic field is 1 kOe, while the applied magnetic field in our manuscript is 100 Oe. The T_B in our manuscript is higher than that in the given reference.
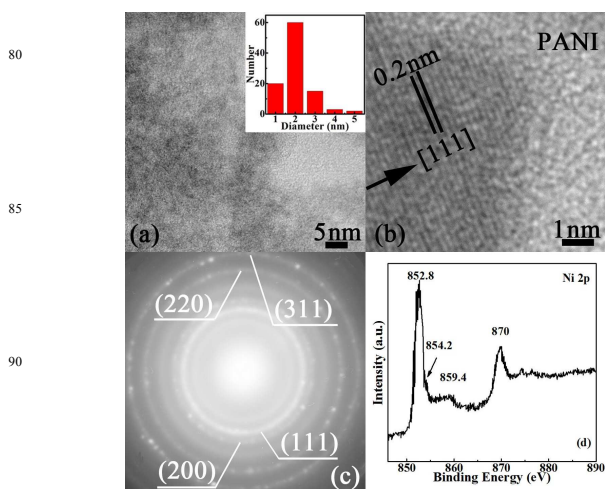
Fig.2. (a)TEM image of Ni@PANI nanocomposites. The inset shows the size distribution of the Ni nanoparticles. (b) A HRTEM image of one Ni nanoparticle. (c) The corresponding SAED and (d) XPS spectrum of Ni2p after etching time of 10 s.
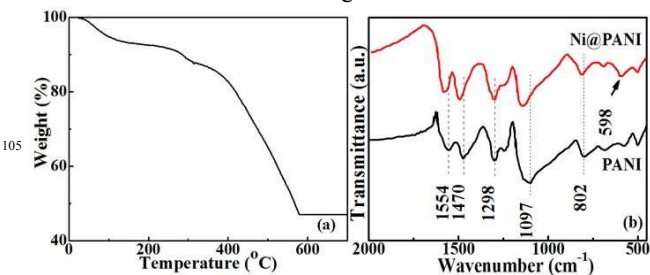
Fig.3. (a) TGA curve of Ni@PANI nanocomposites and (b) FTIR spectra of pure PANI and Ni@PANI nanocomposites.

T_B and the hysteresis loops without coercive force can prove the existence of superparamagnetism. When the nanoparticles are in superparamagnetic state, the magnetic moments of nanoparticles

can randomly flip direction under the influence of temperature, which behavior like paramagnetism. With increasing the applied field, magnetic moments of more and more particles turn to the field direction through the relaxation process. At a certain field, the magnetization of the system gets saturated. When the temperature is higher than the blocking temperature, the fast relaxation processes dominate the magnetic moment rotation, the system can respond immediately to the field change to reach its thermodynamic equilibrium state described by the Langevin function. When the field is decreased to zero, the magnetization will decrease to zero and no coercive force can be observed.[46] Fig.4(b) represents the hysteresis loop recorded at 300 K. The saturation magnetization (M_S) value of Ni@PANI nanocomposite at 300 K is 5.21 emu/g. The M_S of Ni@PANI nanocomposites is 9.5% of the bulk Ni value. The M_S in the present system is larger than that of superparamagnetic Ni@SiO$_2$ nanocomposites.[48] The M_S of Ni@PANI nanocomposites is jointly determined by various factors, such as the content and size of Ni and the antiferromagnetic NiO. The M_S of nanoparticles is lower than that of the corresponding bulk material and is proportional to the nanoparticle sizes, which are often reported in many previous papers.[49, 50] Toshihiko Sato et al reported that saturation magnetization was found to decrease sharply when the particle size was reduced below 10 nm. They proposed the following several possible causes: 1) crystal lattice defects, 2) the mass effect of absorption water on the particles surface, 3) chemical changes on the surface, 4) magnetic degradation of the surface.[49] Sun explained the phenomena by weakly coupled and more disordered spins on the surface.[50] No coercive force can be observed at 300 K because the Ni@PANI nanocomposite is in superparamagnetic state.

The microwave absorption of an absorber highly depends on its EM parameters, i.e., the complex permittivity ($\varepsilon_r=\varepsilon'-j\varepsilon''$) and complex permeability ($\mu_r=\mu'-j\mu''$).[27] In order to investigate the intrinsic reason for microwave absorption properties of the Ni@PANI nanocomposite, the EM parameters are given in Figs.5(a) and 5(b). The real parts (ε' and μ') of ε_r and μ_r stand for the storage of electric and magnetic energy. The imaginary parts (ε'' and μ'') stand for the loss of electric and magnetic energy.[35] As illustrated in Fig. 5(a), besides the peaks located at about 6.6 and 11.4 GHz, the ε' is found to decrease with the frequency increasing from 2 to15.6 GHz, which is consist with the previous reports.[27,51] Wang et al explained this phenomenon by the increased lagging behind of the dipole-polarization response with respect to the electric-field change at higher frequencies.[51] The ε' presents a rapidly decrease in 15.6 - 18 GHz. The ε'' varies from 0.01 to 6.11 in 2-18 GHz with several peaks. The ε'' presents a peak at 16.8 GHz, and approximately equals to 6.12. It can clearly be seen that the value of ε'' exhibit very complex nonlinear behavior.[27] Ni nanoparticle is ferromagnetic metal phase with low dielectric loss and the dielectric performance of nanocomposites is mainly dependent on PANI. According to free-electron theory, $\varepsilon''\approx1/2\pi\varepsilon_0\rho f$, where ρ is the resistivity.[11, 14, 48] The resistivity of Ni@PANI is similar with the nanocomposites with dielectric constituents.[11, 14, 35]

As shown in Fig. 5(b), the value of μ' is around 1 and display week peaks in the frequency range of 2-15.6 GHz, and then rapidly increase to 1.35 at 18 GHz. The value of μ'' has a similar behavior with weak peaks in 2-16 GHz. A strong peak at

around 16.6 GHz is ascribed to the size effect.[10-18] It is worthy noted that the complementary phenomena between ε_r and μ_r exists in the present system, which is similar with the previous report.[12] The complementary behavior is explained by the energy transformation between the permeability and permittivity in the propagation process.[12] The effective refractive index, defined as $n_r=(\varepsilon_r\mu_r)^{1/2}$, is a powerful physical parameter to elevate the energy loss in medium.[12] A larger n_r indicates a stronger electromagnetic attenuation. The modulus of n_r is shown in Fig.5 (c), in which no singularity appears at around16.6 GHz. Zhang et al proposed that the antiresonance behavior of permeability can lead to the additional dielectric loss occurs at around 16.6 GHz.[12] To study the mechanism of magnetic loss, the equation $\mu''(\mu')^{-2}f^{-1}=(2/3)\pi\mu_0d^2\sigma$ is introduced, where d is the thickness of absorber, σ represents the electric conductivity of composite.[47] If the magnetic loss mainly stems from the current eddy, the value of $\mu''(\mu')^{-2}f^{-1}$ is independent of frequency. In Fig. 5(d), the $\mu''(\mu')^{-2}f^{-1}$ varies with the frequency. In addition, hysteresis loss and the domain-wall displacement can be excluded in the ultrasmall superparamagnetic Ni nanoparticles. Therefore, the magnetic loss in the present nanocomposite is caused mainly by the natural resonance.[11, 12]

For a microwave absorption layer, the normalized input impedance at the absorber surface (Z_{in}) is given by $Z_{in}=(\mu_r/\varepsilon_r)^{1/2}\tanh[j(2d/\lambda)(\mu_r\varepsilon_r)^{1/2}]$,with λ the wavelength of microwave in free space and d the thickness of an absorber. The reflection loss (RL) is a function of Z_{in} expressed as: $RL=20\lg|(Z_{in}-Z_0)/(Z_{in}+Z_0)|$.[1-4,52] Applying the experimental ε_r and μ_r into above equations, the RL curves of the Ni@PANI-paraffin nanocomposites can be obtained by using the Matlab procedure. The color map of calculated RL values with the thickness of 1.0-10.0 mm is shown Fig. 6(a). It is worthy noted that the RL values exceeding -20 dB, corresponding to 99% absorption, just locate at the discrete thickness range. From the view of application, the thickness of 2.0 mm is considered to the upper limit of the thickness. Fig. 6(b) exhibits the relationship between the RL values and frequency for the composites with selected thickness in the 1.0-1.3 mm range. The optimal RL value reaches -22.98 dB at 17.8 GHz corresponding to the thickness of 1.0 mm. The effective microwave absorption bandwidth (RL<-10 dB) is 2.4 GHz from 15.6 to 18 GHz. Table 1 shows microwave absorption performance of the representative Ni-based nanocomposites. The superparamagnetic Ni nanoparticles makes the natural frequency shifts to 16.6 GHz and the peak of magnetic loss located at 16.2 GHz. Due to the combined effect of dielectric loss and magnetic loss at 16-18 GHz, the Ni@PANI nanocomposites exhibit the good EM absorption abilities at 16-18 GHz. Compared with the representative Ni-based nanocomposites, ultrasmall superparamagnetic Ni nanoparticles embed in PANI nanocomposites exhibit the thinner thickness and the lower weight percentage in the paraffin-bonded measuring samples. It indicates that the Ni@PANI nanocomposite can be as good candidate for the lightweight and thin microwave absorber.

It is well known that when an EM wave is incident on the surface of an absorber, there are two possible contributions for the EM wave absorption, that is, dielectric loss and magnetic loss.[35] Fig.7 shows the dependence of dielectric loss tangent ($\tan\delta_\varepsilon=\varepsilon''/\varepsilon'$) and magnetic loss tangent ($\tan\delta_\mu=\mu''/\mu'$) on the

frequency in the range of 2-18 GHz.[54] The dielectric loss tangent is larger than the magnetic loss tangent, indicating dielectric loss mainly contributes even more than magnetic loss to microwave absorption for Ni@PANi nanocomposites. Meanwhile, the frequency corresponding to the optimal RL value is in reasonably accord with the peak position of dielectric loss and magnetic loss, which suggest the optimal RL value come from the combined with the dielectric loss and magnetic loss.
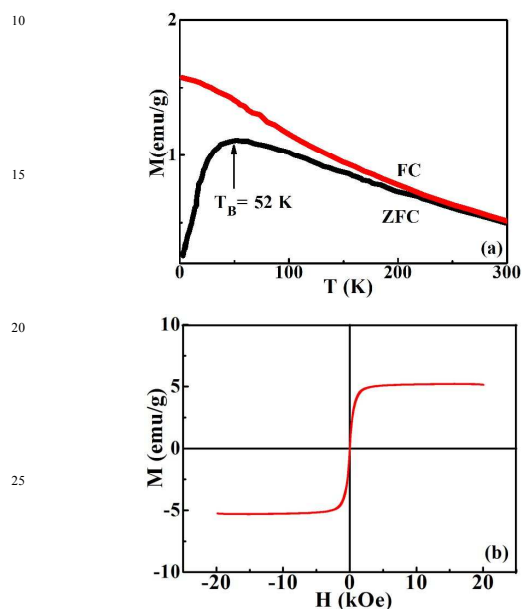
Fig.4. (a) ZFC and FC magnetization curves of the as-prepared Ni@PANI nanocomposite at an applied field of 100 Oe. (b) Magnetic hysteresis loop at 300 K.
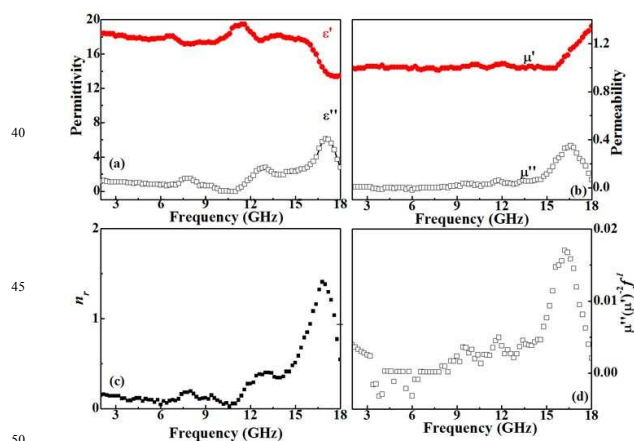
Fig.5. (a) Complex permittivity, (b) permeability, (c) modulus of the effective refractive index and (d) values of $\mu''\mu^{r-2}f^{1}$ as a function of frequency for the paraffin-bonded composite with 25wt% Ni@PANI nanocomposites.

As a result, we can conclude that the ultrasmall superparamagnetic Ni nanoparticles embedded in PANI

nanocomposites with the good EM absorption performances may be originated from some factors, as depicted in inset of Fig.7. At the first stage, the low conductivity of PANI can make most of the EM wave incidence into the nanocomposites by reducing the reflection on the absorber surface. An excellent absorber can attenuate the incident EM wave rapidly through the absorber layer. Secondly, the incidence EM wave is absorbed by the multi-dielectric loss of PANI matrix. Thirdly, due to the size effect of the ultrasmall nanostructure, more interface areas between Ni nanoparticles and PANI matrix can result in the multi-interface polarization effects in the Ni-PANI interface, which play a vital role on the EM wave attenuation. Fourthly, the remanent EM wave into the Ni nanoparticles is further absorbed by the magnetic resonance loss of Ni nanoparticles. Finally, the left EM wave is attenuated through the dielectric loss of PANI matrix again and reduced to an acceptable low magnitude.

Table 1 Microwave absorption of the representative Ni-based nanocomposites.

Samples	wt%	RL(dB)	d(mm)	Ref.
Ni@PANI	50	-35	5.0	18
Ni@C	40	-40	7.8	13
Ni@ZnO	40	-46.9	2.05	11
Ni@SiO₂	50	-49.5	3.5	53
This work	25	-22.98	1.0	
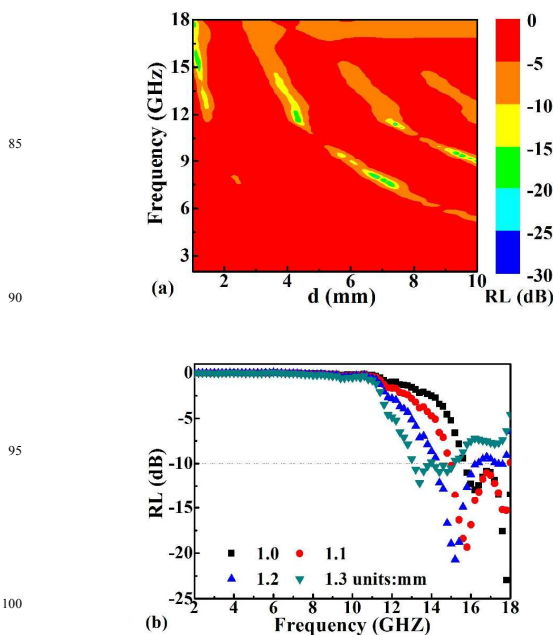
Fig.6. (a) Color map of calculated RL values with the thickness of 1.0-10.0 mm and (b) RL with the selected thickness in 1.0-1.3 mm of the Ni@PANI-paraffin composites as a function of frequency.
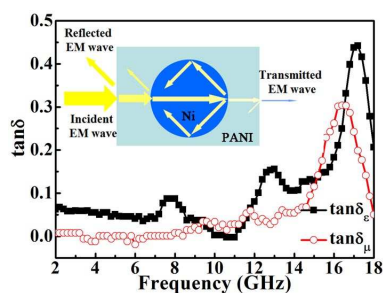
Fig.7. Frequency dependence of the loss tangent for the composites in 2-18 GHz. The inset shows EM wave spread schemes of Ni@PANI nancomposites.

Conclusions

In conclusion, superparamagnetic Ni nanoparticles embedded in PANI nanocomposites were prepared by a simple oxidation-reduction method followed by an in situ polymerization process. The microstructure and magnetic properties of Ni@PANI nanocomposites were investigated in detail. The Ni nanoparticles with single crystalline and single magnetic domain structure possess the average diameter of ~2.1 nm. The T_B of Ni@PANI nanocomposites is established to be 52 K and no coercive force was observed at 300 K, indicating the Ni@PANI nanocomposites are superparamagnetic at 300 K. Paraffin-bonded composites with 25 wt% Ni@PANI nanocomposites were further evaluated as the lightweight and thin microwave absorber. The optimal RL value of Ni@PANI-paraffin composites reaches -22.98 dB at 17.8 GHz corresponding to the thickness of 1.0 mm. Compared with the represented Ni-based nanocomposites, Ni@PANI nanocomposites with the favorable properties in a lower density and thinner thickness result from the combined effect of magnetic loss and dielectric loss by introducing ultrasmall superparamagnetic Ni nanoparticles into PANI matrix. This work suggests that the ultrasmall superparamagnetic Ni nanoparticles embedded in PANI nanocomposistes can be used as lightweight and thin EM absorber.

Acknowledgements

Notes and references

aCollege of Science, Northeast Dianli University, Jilin 132012, PR China. Fax/Tel:+86 432 64806631; E-mail: loveh_andan@163.com
bCollege of Science, Tianjin Polytechnic University, Tianjin, 300387, PR China.
cCollege of Instrumentation & Electrical Engineering, Jilin University, 130021, PR China.

† Electronic Supplementary Information (ESI) available: See DOI: 10.1039/b000000x/

1 X.F. Zhang, P.F. Guan and J.J. Guo, Part. Part. Syst. Charact. 2013, 30, 842-846.
2 J.J. Jiang, D. Li, D.Y. Geng, J. An, J. He, W. Liu and Z.D. Zhang, Nanoscale 2014, 6, 3967-3971.
3 X.G. Liu, N.D. Wu, C.Y. Cui, N.N. Bi and Y.P. Sun, RSC Adv. 2015, 5, 24016-24022.
4 N.N. Bi, X.G. Liu, N.D. Wu, C.Y. Cui and Y.P. Sun, RSC Adv. 2015, 5, 32452-32459.
5 Y. Li, J. Zhang, Z.W. Liu, M.M. Liu, H.J. Lin and R.C. Che, J. Mater. Chem. C 2014,2, 5216-5222.
6 H.Y. Miao, J.H. Liu and L. Saravanan, J. Phys. D: Appl. Phys. 2015, 48, 215301.
7 W.X. Li, L.C. Wang, G.M. Li and Y. Xu, J. Alloys Compd. 2015, 633, 11-17.
8 C.C. Lee and D.H. Chen, Appl. Phys. Lett. 2007, 90, 193102.
9 R.C. Che, L.M. Peng, X.F. Duan, Q. Chen and X.L. Liang, Adv. Mater. 2004, 16, 401-405.
10 B. Lu, X.L. Dong, H. Huang, X.F. Zhang, X.G. Zhu, J.P. Lei and J.P. Sun, J. Magn. Magn. Mater. 2008, 320, 1106-1111.
11 X.G. Liu, J.J. Jiang, D.Y. Geng, B.Q. Li, Z. Han, W. Liu and Z.D. Zhang, Appl. Phys. Lett. 2009, 94, 053119.
12 X.F. Zhang, P.F. Guan and X.L. Dong, Appl. Phys. Lett. 2010, 97, 033107.
13 H. Wang, Y.Y. Dai, W.J. Gong, D.Y. Geng, S. Ma, D. Li, W. Liu and Z.D. Zhang, Appl. Phys. Lett. 2013, 102, 223113.
14 Z. Han, D. Li, H. Wang, X.G. Liu, J. Li, D.Y. Geng and Z.D. Zhang, Appl. Phys. Lett. 2009, 95, 023114.
15 J.J. Jiang, H. Wang, H.H. Guo, T. Yang, W.S. Tang, D. Li, S. Ma, D.Y. Geng, W. Liu and Z.D. Zhang, Nano. Res. Lett. 2012, 7, 238.
16 Z.H. Wang, X. He, X. Wang, Z. Han, D.Y. Geng, Y.L. Zhu and Z.D. Zhang, J. Phys. D: Appl. Phys. 2010, 43, 495404.
17 X.G. Liu, C. Feng, S.W. Or, Y.P. Sun, C.G. Jin, W.H. Li and Y.H. Lv, RSC Adv. 2013, 3, 14590-14594.
18 X.L. Dong, X.F. Zhang, H. Huang and F. Zuo, Appl. Phys. Lett. 2008, 92, 013127.
19 T.C. Zou, H.P. Li, N.Q. Zhao and C.S. Shi, J. Alloys Compd. 2010, 496, L22-L24.
20 C.C. Lee and D.H. Chen, Appl. Phys. Lett. 2007, 90, 193102.
21 T.T. Chen, F. Deng, J. Zhu, C.F. Chen, G.B. Sun, S.L. Ma and X.J. Yang, J. Mater. Chem. 2012, 22, 15190-15197.
22 Z.B. Li, Y.D. Deng, B. Shen and W.B. Hu, Mater. Sci. Eng. B 2009, 164, 112-115.
23 C.D. Pina, A.M. Ferretti, A. Ponti and E. Falletta, Compos. Sci. Technol. 2015,110, 138-144.
24 J.Y. Cheng, B. Zhao, S.Y. Zheng, J.H. Yang, D.Q. Zhang and M.S. Cao, Appl. Phys. A 2015,119, 379-386.
25 A. Ohlan, K. Singh, A. Chandra and S.K. Dhawan, ACS Appl. Mater. Interf. 2010, 2, 927-933.
26 Y.B. Li, G. Chen, Q.H. Li, G. Z. Qiu and X.H. Liu, J. Alloys Compd. 2011, 509, 4104-4107.
27 Y. Xu, J.H. Luo, W. Yao, J.G. Xu and T. Li, J. Alloys Compd. 2015,636, 310-316.
28 Y. Ma, M.T. Qiao, Y.H. Chen, C.P. Hou, B.L. Zhang and Q.Y. Zhang, RSC Adv. 2015,5, 9986-9992.
29 L.W. Jiang, Z.H. Wang, D. Li, D.Y. Geng, Y. Wang, J. An, J. He, W. Liu and Z.D. Zhang, RSC Adv. 2015, 5, 40384-40392.
30 J. Zhao, J.P. Lin, J.P. Xiao and H.L. Fan, RSC Adv. 2015, 5, 19345-19352.
31 M. Wang, G.B. Ji, B.S. Zhang, D.M. Tang, Y. Yang and Y.W. Du, J. Magn. Magn. Mater. 2015, 377, 52-58.
32 F.F. Xu, L. Ma, Q.S. Huo, M.Y. Gan and J.H. Tang, J. Magn. Magn. Mater. 2015, 374, 311-316.
33 B.H. Kim, M.J. Hackett, J. Park and T. Hyeon, Chem. Mater. 2014, 26, 59-71.
34 T. Jaumann, E.M.M. Ibrahim, S. Hampel, D. Maier, A. Leonhardt and B. Büchner, Chem. Vap. Deposition 2013, 17, 1-7.
35 X.G. Liu, Z.Q. Ou, D.Y. Geng, Z. Han, Z.G. Xie and Z.D. Zhang, J. Phys. D: Appl. Phys. 2009, 42, 155004.
36 C.P. Wang, C.H. Li, H. Bi, J.C. Li, H. Zhang, A.J. Xie and Y.H. Shen, J. Nanopart. Res. 2014, 16, 2289.
37 U. Holtwarth and N. Gibson, Nature Nanotech. 2011, 6, 534-534.
38 K. Kishi and T. Fujita, Surf. Sci. 1990, 227, 107-113.
39 L.S. Hsu and R.S. Williams, J. Phys. Chem. Solids 1994, 55, 305-312.
40 M.G. Thube, S.K. Kulkarni, D. Huerta and A.S. Nigavekar, Phys.Rev. B 1986, 34, 6874-6877.
41 N.S. McIntyre, T.C. Chan and C. Chen, Oxid. Met. 1990, 33, 457-479.

42 F. Ye, B. Zhao, R. Ran and Z.P. Shao, J. Power Sources 2015, 290, 61-70.

43 X.F. Wang, Y.H. Shen, A.J. Xie, S.K. Li, Y. Cai, Y. Wang and H.Y. Sun, Biosens. Bioelectron. 2011, 26, 3063-3067.

5 44 Y.P. Sun, F. Xiao, X.G. Liu, C. Feng and C.G. Jin, RSC Adv. 2013, 3, 22554-22559.

45 E.M.M. Ibrahim, S. Hampel, J. Thomas, D. Haase, A.U.B. Wolter, V.O. Khavrus, C. Täschner, A. Leonhardt and B. Büchner, J. Nanopart. Res. 2012, 14, 1118.

10 46 S. Ma, Y.B. Wang, D.Y. Geng, J. Li and Z.D. Zhang, J. Appl. Phys. 2005, 98, 094304.

47 X.X. Zhang, Magnetic relaxation and quantum tunneling of magnetization, Handwork of Advanced Magnetic Materials, 2006.

48 F.C. Fonseca, G.F. Goya and R.F. Jardim, Phys. Rev. B 2002, 66, 15 104406.

49 T. Sato, T. Iijima, M. Seki and N. Inagaki, J. Magn. Magn. Mater. 1987, 65, 252-256.

50 C.Q. Sun, Prog. Solid State Chem. 2007, 35, 1-159.

51 H. Wang, H.H. Guo, Y.Y. Dai, D.Y. Geng, Z. Han, D. Li, T. Yang, S. 20 Ma, W. Liu and Z.D. Zhang, Appl. Phys. Lett. 2012, 101, 083116.

52 S.L. Wen, Y. Liu, X.C. Zhao and Z.Z. Fan, J. Mag. Mag. Mater. 2015, 385, 182-187.

53 B.C. Wang, T. Wang, L. Qiao and F.S. Li, Adv. Mater. Res. 2011, 160-162, 945-950.

25 54 X.G. Liu, B. Li, D.Y. Geng, W.B. Cui, F. Yang, Z.G. Xie, D.J. Kang and Z.D. Zhang, Carbon 2009, 47, 470-474.